Edge selection and sparse representation based motion deblurring method

Xixuan Zhao, Jiangming Kan*

***Abstract*—**Motion deblurring has long been a challenging yet fundamental problem in image processing. In this paper, we address the problem of blind motion deblurring by incorporating global priori information, kernel priori information and sparse representation in a unified framework. Then, we alternately solve the estimated kernel and the deblurred image. To obtain a more accurate blurring kernel, we propose an edge selection step to select useful edges for kernel estimation and introduce an intermediate image to improve the accuracy of kernel estimation.

Experimental results show that the proposed method runs fast and achieves comparable results to those of the state-of-the-art algorithms. Sometimes, this proposed method outperforms these other algorithms in both synthetic and real-world image experiments.

***Keywords*—**motion deblurring; edge selection; sparse representation

I. Introduction

Motion blurs occur frequently in digital photography, usually caused by camera shake. Methods for motion deblurring have been extensively investigated as it has long been a fundamental and important problem in computer vision. According to whether the blurring kernel is known, research can be classified into blind and non-blind deconvolution. In most of the real-world cases, we have no knowledge of the exact blurring kernel. Therefore, in our study, we focus on blind deconvolution algorithms. As it is an ill-posed problem, the regularization technique is primarily used to deal with it.

Many studies focus on the use of various priors to construct regularization cost function. Fergus et al. [1] proposed a Gaussian model to approximate the heavy-tailed gradient distributions in natural images and use it as regularization for recovering images. Shan et al. [2] introduced the global prior and local prior of natural images in recovery process, and adopted a two piece-wise continuous function to fit the heavy-tailed gradient distributions. Krishnan et al. [3] proposed a hyper-Laplacian distribution that usually outperformed the former two and was used extensively in subsequent works. The alternating minimization technique, originally proposed by Geman et al. [4, 5], is extensively used to solve the above cost function optimization problem. Iterative estimation can avoid being stuck in local minima, but it has the problem of dense kernel and visual artifacts.

To obtain a more accurate kernel, recently studies have found that salient edge selection is also an important factor that affects reliable kernel estimation [6]. Cho and Lee [7] adopt bilateral filtering with shock filtering to predict strong edges. Xu and Jia [8] proposed a metric to select useful edges. They found that salient edges do not always help kernel refinement, and bad selection may mistake kernel estimation. Joshi et al. [9] proposed an applicable method for predicting a sharp image from a single blurry image. These methods show superior performance during kernel estimation.

Dictionary learning and sparse representation techniques are recent hot topics in blind image restoration. Li et al. [10] deblurred images via an adaptive dictionary learning strategy. Yin [10] et al. [11] found that there exists a coupled sparse representation between the blurred and sharp image patch pairs under their own dictionaries. Elad et al. [12] constructed a dictionary based on large numbers of natural images and the blurred image itself. They then solved the proposed sparsity regularization cost function using the KSVD algorithm, which performs excellently during denoising and signal recovery.

However, in dictionary learning and sparse representation techniques, large images are divided into small patches to process, and thus, there inevitably exist boundary artifacts. To overcome this problem and acquire a more precise estimated kernel, we propose an edge selection step to select useful edges for kernel estimation. We then incorporate the kernel estimation process in an image restoration framework in order to effectively restrain the noise and boundary artifacts. Experimental results demonstrate the effectiveness and speed of the proposed method.

II. Our model

A. Blurring model

By convention, we assume the formation model of a blurred image Y as a sharp image blurred by a blurring kernel K along with random noise n:

$$Y = K \otimes X + n \tag{1}$$

We observe the blurred image Y. Our goal is to recover the unknown sharp image X and the blurring matrix K by fully using the information of Y. This is a blind image restoration

This work is supported by the National Natural Science Foundation of China (Grant No. 31570713) and the Fundamental Research Funds for the Central Universities (Grant No. TD2013-4)

Xixuan Zhao, Jiangming Kan are with the Beijing Forestry University, Beijing 100083, China. (corresponding author phone: 010-62336137-706; e-mail: kanjm@bjfu.edu.cn).

problem that is typically underdetermined. To solve this problem, a regularization method containing prior information is primarily used to acquire the solution, and it can be expressed as

$$\{\hat{\mathrm{X}},\hat{\mathrm{K}}\}=\arg\min\left\|\mathrm{K}\otimes\mathrm{X}-\mathrm{Y}\right\|_2^2+\mu\phi(X)+\beta\rho(K) \quad (2)$$

where $\phi(X)$ denotes a regularization item containing prior information of sharp natural images and $\rho\ (K)$ represents a kernel regularization item. μ,β are regularization parameters that control the weights of the regularization items. $\otimes$ denotes the convolution operation. In the following paragraphs, we will introduce the detail composition of the sharp image prior regularization item $\phi(X)$ and the kernel constraints prior regularization item $\rho(K)$.

B. Sharp image prior regularization item

In our proposed method, the sharp image prior $\phi(X)$ consists of two parts, sparse representation prior and global gradient prior.

Sparse representation is helpful in image processing and present state-of-the-art performance for image denoising. We consider it to take advantages of such a sparse representation model. Usually, in a sparse model, the image is divided into small image patches to quickly realize the sparse representation and reconstitution process. It is based on the assumption that all image patches can be adequately approximated by a sparse linear combination of a learned patch dictionary [11]. Our optimization form for the sparse representation prior is defined as

$$\min\eta\left\|X-\sum_i R_i D\alpha_i\right\|_2^2+\lambda\sum_i\left\|\alpha_i\right\|_1 \quad (3)$$

where R_i maps the ith non-overlapping patch to the corresponding position in the image, η, λ are the weights and α_i denotes the representation coefficients of non-overlapping patches. Here, the first item ensures the proximity of sparse reconstruction and the second term restrains the sparsity of the sparse coefficient.

As mentioned above, we divide the image into small non-overlapping image patches to quickly realize sparse representation. This will lead to the problem of lacking smoothness constraints between non-overlapping patches and can easily cause severe artifacts along the boundaries [12, 13]. To address this problem, we introduce the hyper-Laplacian prior as the global gradient prior, and the optimization form of it is defined as

$$\min\tau\sum_i\left|\nabla X\right|^{2/3} \quad (4)$$

where ∇X represents the vertical and horizontal spatial gradients of the image and τ is the parameter to control the weight. This global gradient prior assumes a hyper-Laplacian distribution of gradients in natural scenes [3]. Constraining the distribution in the blurred image can enforce smoothness between nearby pixels and thus can alleviate artifacts along the boundaries.

According to the previously mentioned analysis, we obtain our sharp image prior regularization items as:

$$\phi(X)=\eta\sum_i\left\|R_iX-D\alpha_i\right\|_2^2+\lambda\sum_i\left\|\alpha_i\right\|_1+\tau\sum_i\left|\nabla X\right|^{2/3} \quad (5)$$

C. Kernel constraints prior regularization item

We define the kernel constraints prior as:

$$\rho\ (K)=\gamma\left\|K\right\|_2^2 \quad (6)$$

This term can efficiently preserve the sparsity. It will penalize large gradients and thus bias the kernels to take on values similar to their neighbors [9]. K is subject to the constraints $k\geq 0,\sum_i k_i=1$ as well.

D. Target cost function

Here, as $\phi(X)$ and $\rho\ (K)$ are incorporated in our method for optimization, we finally obtain our target cost function as:

$$\begin{aligned}E(X,K)&=\left\|K\otimes X-Y\right\|_2^2+\mu\phi(X)+\beta\rho(K)\\&=\left\|K\otimes X-Y\right\|_2^2+\eta\sum_i\left\|R_iX-D\alpha_i\right\|_2^2\\&+\lambda\sum_i\left\|\alpha_i\right\|_1+\tau\sum_i\left|\nabla X\right|^{2/3}+\gamma\left\|K\right\|_2^2\end{aligned} \quad (7)$$

Directly optimizing (7) is hard, since there are lots of unknown variables and they can regularly exhibit poor convergence. We optimize E by iteratively estimating K, X and α. We employ a set of advanced optimization techniques to solve specific problems in the process.

III. Optimization

A. Edge Selection-Based Blind Kernel Estimation

First, we fix X and α to optimize K. Then, the cost function E can be simplified to:

$$\min_{\{\mathrm{k}\}}\left\|K\otimes X-Y\right\|_2^2+\gamma\left\|K\right\|_2^2 \quad (8)$$

As the estimation accuracy of the kernel has a strong influence on sharp image recovery, we preprocess the image and introduce an intermediate image to alternate estimating the kernel in a multi-scale framework.

The existence of noise will greatly influence the recovery image. Thus, first, we use bilateral filtering to handle the noise. Bilateral filtering is a nonlinear filtering method that has the advantage of preserving high-frequency information while denoising and thus can preserve edge information for kernel estimation.

Then, we use shock filter to construct sharp edges to guide the global image restoration. Shock filter can effectively improve the image features and help to recover sharp edges from a blurred image. The Shock filtering process can be expressed by the following mathematical model

$$X_{t+1} = X_t - sign(\Delta X_t)\|\nabla X_t\|dt \tag{9}$$

where X_t denotes the t th iteration of the image and ∇X_t and ΔX_t denotes the first-order derivative and the second derivative of X_t respectively. In our proposed method, we use first-order edge detection operator and Laplace operator for calculation. dt is the step size.

Operated by Shock filter, the image will have obvious, rich edges. Research from [8] has shown that insignificant edges make kernel estimation vulnerable to noise, and some even inaccurately estimate kernels. Therefore, the present paper innovatively proposes an edge selection method to select qualified edges for kernel estimation.

First, we switch to polar coordinates and divide the image into four areas according to the gradient direction angle as $\frac{\pi}{4}$, $\frac{\pi}{2}$, $\frac{3\pi}{4}$, π. In each area, we pick m edges of the largest gradient magnitude by following criterion

$$m = \max(\sqrt{N_1 N_k}/20, 10) \tag{10}$$

where N_I and N_k denote the number of total pixels in the current image area and kernel. We denote our selected map edges as ∇X^m and use it as the basis for kernel estimation. Then, we transform the objective function (8) to

$$\min\left\|\nabla X^m \otimes K - \nabla Y\right\|_2^2 + \gamma\left\|K\right\|_2^2 \tag{11}$$

We take the derivative with respect to K and set it equal to zero to solve the minimization problem. Based on Parseval's theorem, we perform FFTs on all variables to transform the convolution operation in the time domain to multiplications in the frequency domain. Thus, we greatly reduce the amount of calculations, and have

$$k = \mathcal{F}^{-1}\left(\frac{\overline{\mathcal{F}(\partial_x X^m)}\mathcal{F}(\partial_x Y) + \overline{\mathcal{F}(\partial_y X^m)}\mathcal{F}(\partial_y Y)}{\mathcal{F}(\partial_x X^m)^2 + \mathcal{F}(\partial_y X^m)^2 + \gamma}\right) \tag{12}$$

where ∂_x, ∂_y represents the horizontal and vertical gradient operator. $\mathcal{F}(.)$ and $\mathcal{F}^{-1}(.)$ denote the *FFT* and inverse *FFT* respectively. $\overline{\mathcal{F}(.)}$ is the complex conjugate operator.

Considering that the blurring kernel caused by motion should have a single, connected structure that has the feature of sparsity, we refine the blurring kernel by eliminating the small, negative value of the estimated kernel, only keeping one mostly connected structure, and regularizing it to keep image energy constant.

Large blurring kernels usually cause broad edges of the image. In this case, only using shock filter is not enough. We address this problem by using a multi-scale framework based on the fact that when we reduce the scale of image the width of the blurred edges become sharper as well; then, shock filter can play an effective role.

Therefore, we introduce an intermediate image in order to alternatively estimate the kernel in a multi-scale framework. We use the selected sharp edges ∇X^m to construct the objective function to acquire an intermediate image

$$\hat{X}_{in} = \arg\min_X \left\|K \otimes X - Y\right\|^2 + \kappa\left\|\nabla X - \nabla X^m\right\|^2 \tag{13}$$

where the first term denotes the global reconstruction error, the second term is a spatial prior which does not blindly enforce small gradients near strong edges and thus allows for a sharp recovery. These two terms prove to be useful in solving our problem [14]. κ is the regularization weight, which is set as $2e^{-3}$.

In the frequency domain, we process a few algebraic operations and get the closed-form solution:

$$\hat{X}_{in} = \mathcal{F}^{-1}\left(\frac{\overline{\mathcal{F}(k)}\mathcal{F}(Y) + \kappa(\overline{\mathcal{F}(\partial_x)}\mathcal{F}(X_x^s) + \overline{\mathcal{F}(\partial_y)}\mathcal{F}(X_y^s))}{\overline{\mathcal{F}(k)}\mathcal{F}(k) + \kappa(\overline{\mathcal{F}(\partial_x)}\mathcal{F}(\partial_x) + \overline{\mathcal{F}(\partial_y)}\mathcal{F}(\partial_y))}\right) \tag{14}$$

We alternate between estimating the kernel and the intermediate image in a multi-scale framework to acquire a finer kernel estimation result. We use a coarse-to-fine pyramid of image resolution, in a similar manner as in [15]. We set the size ratio at $\sqrt{2}$ between each level where the number of levels can be adjusted by the size of K. We set kernel size at the coarsest level as 3×3 and perform $q = 2$ alternating updates of $\hat{X}_{in}$ and K. The overall kernel estimation process is shown as Algorithm 1.

Algorithm 1 Kernel estimation process

1.**Input**: blurred image Y, regularization parameters γ, κ, iteration numbers q.

2.**Initialization**: K_0, $X_0 = Y$

3. **for** $i = 1:4$ (For four levels of downsampling)

4. Acquisition of needed edges in current level ∇X_i^m:

Preprocessing of X_i by bilateral filtering, (9) and (10).

5.**for** $j = 1 \to q$ **do**

Solve for K_i by minimizing model (11)

Solve for $\hat{X}^i_{in}$ by minimizing model (13)

end for

Downsample $\hat{X}^i_{in}$ to form the new input X_{i+1}

end for

6. **Output**: Estimated kernel K.

B. α estimation

In this part, we fix X and K to optimize α. Then, the cost function E can be simplified in the following form

$$\min_{\{\alpha_i\}} \eta \sum_i \|R_i X - D\alpha_i\|_2^2 + \lambda \sum_i \|\alpha_i\|_1 \quad (15)$$

which can further decompose into smaller problems for each patch

$$\min_{\alpha_i} \eta \|X_i - D\alpha_i\|_2^2 + \lambda \|\alpha_i\|_1 \quad (16)$$

where X_i denotes the i^{th} patch of the image and α_i is the representation coefficients of each non-overlapping patch. Then, the problem turn into a l_1 norm optimization problem. Algorithms to solve this kind of problem have been extensively investigated. In our proposed method, we use the LARS method to find the solution. [16]

C. X estimation

We fix the value of α and k to estimate the recovery image X. Then, the solution of cost function E can be simplified by solving the non-convex problem:

$$\min_{\{X\}} \|K \otimes X - Y\| + \eta \sum_i \|R_i X - D\alpha_i\|_2^2 + \tau \sum_i |\nabla X|^{2/3} \quad (17)$$

Using the half-quadratic penalty method [3], we introduce an auxiliary variable Z that allows us to move the derivative operator ∇ out of the $l_{2/3}$ expression, thus enabling us to find the optimal X. The new cost function turns to

$$\min \|K \otimes X - Y\| + \eta \sum_i \|R_i X - D\alpha_i\|_2^2 + \upsilon \|\nabla X - Z\|_2^2 + \tau \sum_i |Z|^{2/3} \quad (18)$$

Here, as $\upsilon \to \infty$ during the optimization, the solution to (18) will converge to that of (17). In practice, it is not necessary to achieve convergence for each fixed υ and one iteration of update will be sufficient [17]. We fix a υ, then minimize (18) by alternating between optimizing X and Z.

① Given a fixed Z and υ, we conduct 2D Fast Fourier Transform (FFT) on (18) to diagonalize K and ∇. For simplicity, we set $U = \sum_i D\alpha_i$. We then have

$$(K^T K + \eta I + \upsilon \nabla^T \nabla) f = K^T Y + \eta U + \upsilon \nabla^T Z \quad (19)$$

After collating (19) we have the optimal X:

$$\tilde{x} = \mathcal{F}^{-1}\left(\frac{\mathcal{F}(k)^* o \mathcal{F}(\tilde{y}) + \beta \mathcal{F}(\tilde{u}) + \alpha \mathcal{F}(d)^* o \mathcal{F}(\tilde{z})}{\mathcal{F}(k)^* o \mathcal{F}(k) + \beta + \alpha \mathcal{F}(d)^* o \mathcal{F}(d)}\right) \quad (20)$$

Here, we define $\hat{x}, \hat{z}, \hat{u}$ as the 2D form of X, Z, U and k, d as the corresponding 2D convolution kernel to K, ∇. Equation (20) only involves several multiplication processes and thus, can be calculated rapidly.

② Given a fixed X and υ, the cost function can then be optimized by minimizing each component:

$$\hat{Z} = \min_{(Z)_j} \upsilon \sum_j \left|(\nabla X - Z)_j\right|^{2/3} + \tau \sum_j \left|(Z)_j\right|^{2/3} \quad (21)$$

We take the derivative of Z and collate the equation, so we have:

$$Z^4 - 3(\nabla \hat{X}) Z^3 + 3(\nabla \hat{X})^2 Z^2 - (\nabla \hat{X})^3 Z + \frac{\tau^3}{27\upsilon^3} = 0 \quad (22)$$

Using the analytic method provided in [3], we can quickly get a root of (22) which is the solution of Z.

D. Summary of algorithm

To summarize our proposed method, we present the pseudocode of the overall optimization framework as Algorithm2. We minimize the overall target cost function (7) by alternating solving the target variables. Fig.1 gives a visual example of the estimation process of our proposed method.

Algorithm 2 Overall optimization framework of our proposed method

1.Input:blurred image Y, regularization parameters $\eta, \lambda, \tau, \gamma$, Iteration number $t = 3$.

2.Initialization: K_0, X_0, α_0

3.for $i = 1 \to t$ **do**

Solve for K according to Algorithm 1;
Solve for α by minimizing model (15);
Solve for X by minimizing model (17);

end for

4.Output: Deblurred image X, estimated kernel K.

(a) (b) (c)

(d) (e) (f)

Fig.1 Estimation process: (a) Blurred image (b) Extracted edges of bilateral filtering image (c) Shock filtering image (d)Extracted edges of shock filtering image (e) Selected edges by our proposed method (f) deblurred image

IV. Experimental Results

In the experiments, as color images can be easily processed by a simple concatenation of values of each RGB channel, we

work on gray-scale images that can reduce the computational complexity while testing the efficiency of the proposed method. All experiments are conducted on the same PC with an Intel(R) Pentium(R) CPU and 4GB memory.

In practice, we set the parameters in (7) as $\eta = 200, \lambda = 2.5, \tau = 2.5, \gamma = 10$ and use 12×12 patches with 8 pixels overlapped to conduct the sparse representation. The dictionary provided by [13] is trained from the Berkeley Segmentation database with a size of 144×577.

We conduct experiments on both synthetic motion blur images and real-world blurred images to verify the effectiveness of our proposed method. This also allows us to compare its deblurring ability with publicly available, state-of-art deblurring algorithms, including algorithms proposed by Krishnan et al. [15], Xu et al. [18], Pan et al. [19] and Bioucas-Dias et al. [20]. To be fair, we set the parameters of these algorithms according to their corresponding papers to ensure best performance.

A. Experiments on synthetic motion blur image

In this section, we adopt synthesized blurred images as test images. As the base of a synthetic motion blurred image is known, we adopt a quantitative comparison index to evaluate performance. PSNR is widely used as an evaluation index, but many experimental results show that it is inconsistent with the visual quality of human eyes [21]. Therefore, we choose structural similarity (SSIM) as the evaluation index, under which a higher value represents a better restoration result. The SSIM index is defined as

$$SSIM(x,y) = \frac{(2\mu_x\mu_y + C_1)(2\sigma_{XY} + C_2)}{(\mu_x^2 + \mu_y^2 + C_1)(\sigma_x^2 + \sigma_y^2 + C_2)} \quad (23)$$

where μ_x, σ_x and σ_{xy} are the mean, the variance of x and the covariance of x and y, respectively. C_1 and C_2 are constants given by 2.55^2 and 7.65^2, respectively. Here, x and y are patches extracted from the same spatial location from the recovery image and the ground truth image.

For our first experimental set, the test image is blurred by the four different blurring kernels shown in Fig.2 to obtain the degraded images. Kernel1 is set to be a motion blurred kernel (direction 135^o with motion length 21). Kernel 2 and Kernel 3 are two custom, complex blurring kernels that can efficiently test the stability of algorithms. Kernel4 is a Gaussian blurred kernel with standard derivation $\sigma = 2$ pixels.

Kernel 1 Kernel 2 Kernel 3 Kernel 4

Fig.2 Blurring kernels

We use three classical images --"Lena", "Cameraman" and ''Peppers'' as the original test images. The average SSIM value comparison of the deblurred images acquired by our proposed method and the other three comparison methods under these four blurring kernels are shown in Table 1. According to these results, our proposed method performs significantly better than the other methods for synthetic motion blur images with an average SSIM value more than 0.8.

Table1 Deblurring result comparison under different kernels (additive no noise)

SSIM	Krishnan et al.[15]	Xu et al.[18]	Pan et al.[19]	Ours
Kernel1	0.74688	0.79091	0.79702	0.8215
Kernel2	0.72478	0.65568	0.67082	0.81467
Kernel3	0.64349	0.71887	0.75554	0.82013
Kernel4	0.83828	0.82043	0.81484	0.83142

In order to intuitively compare the estimated kernels, we give a visual comparison example of the estimated kernel generated by our method and other available methods in Fig.3. The estimated kernel of our proposed method is clear and accurate compared to the ground truth in Fig.2 and has clearer structures and less impurity than the comparative methods.

(a)Estimation results by Krishnan et al. [15]

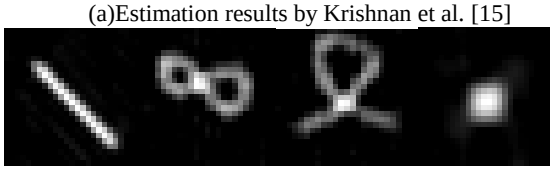

(b)Estimation results by Pan et al. [19]

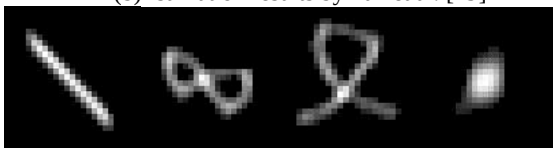

(c)Estimation results of our proposed

Fig.3 Kernel estimation results

To compare the algorithm speed, we record the average running time of our algorithm and the other three comparative methods in Table 2, from which we see that our proposed method is more efficient and faster.

Table 2 Time consumption comparison

Algorithm	Krishnan et al.[15]	Xu et al.[18]	Pan et al.[19]	Ours
Average time (s)	70.270	110.721	500.342	28.517

To further evaluate the anti-noise performance of the proposed method, we conduct our experiments on test images that are blurred and add random Gaussian noise. We increase the noise gain and observe the SSIM value of the deblurred

images from different methods.

The changing curves of the SSIM value with noise gain are shown in Fig.4. We plot it until the SSIM values of the deblurred images are lower than the original blurred images. As can be observed, Xu's method is declining rapidly with increasing noise gain, which shows a relatively poor anti-noise performance while our proposed method shows a stable anti-noise performance and better deblurring ability with the highest SSIM value.

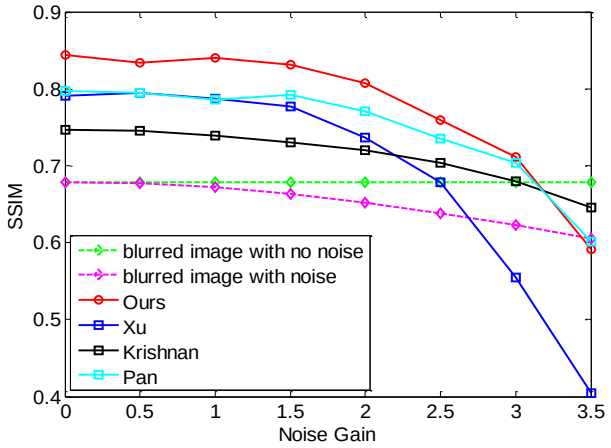

Fig.4 Anti-noise performance illustration. We plot the changing curves of SSIM value with noise gain.

B. Experiments on real-world blurred images

In this section, we conduct experiments on real-world blurred images with different sizes and blurring levels presented in other deblurring works. To quantitatively compare and evaluate the deblurring ability, we employ NIQE, a blind image quality analyzer proposed in [22], to measure the performance of different methods. Analyses in [21] demonstrate the effectiveness of NIQE in evaluating real-world deblurred images.

In Fig.5, we show an example from [8] that contains relatively dense edges and noisy points. From the final deconvolved images from different methods we can see that Bioucas-Dias's and Krishnan's method shows good anti-noise performance as the three noisy points at the bottom right reduce less image quality. However, our proposed method shows a higher quality of recovering edges and structures, and we can observe obviously clearer letters than the results of other deblurring methods. The NIQE evaluation results in Table3 show the priority of our proposed method as well.

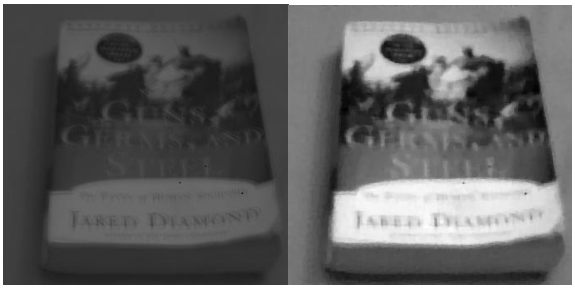

(a)Blurred image (b) Bioucas-Dias et al.[20]

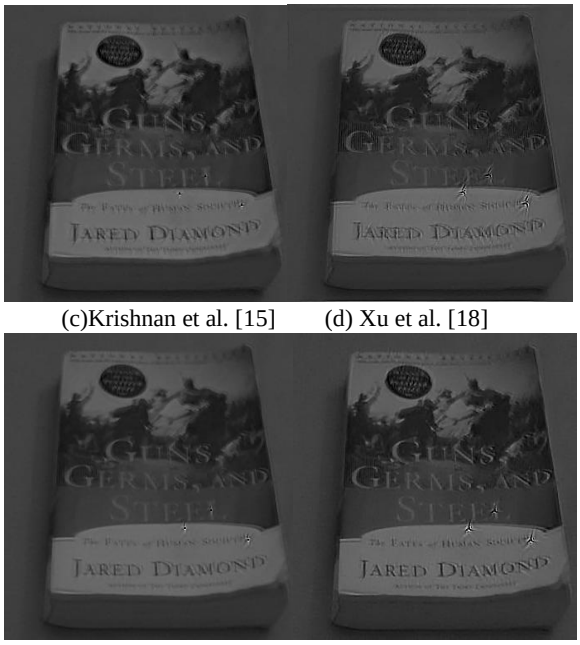

(c)Krishnan et al. [15] (d) Xu et al. [18]

(e) Pan et al. [19] (f)Ours

Fig.5 Deblurred results of image "Book" using different methods

Table 3 NIQE evaluation results of test images by different methods

	Bioucas Dias[20]	Krishnan et al.[15]	Xu et al.[18]	Pan et al.[19]	Ours
Book	4.7818	5.2969	4.8355	5.255	5.4816
House	4.4576	4.0764	3.9665	4.8206	7.0263
Building	3.6268	3.9476	4.3329	5.9769	5.8945

In Fig.6, another example with clear boundaries and small blurring kernel from [18] is shown. From visual perspective, the results of [20],[15] and [18] show "a layer of mist". Our proposed method and [19] show a visually plausible results, while our proposed method gives sharper "window edges" of the image. The NIQE evaluation results shown in Table 3 are in accordance with this analysis, which demonstrates the effectiveness of our proposed method.

(a)Blurred image (b) Bioucas-Dias et al.[20]

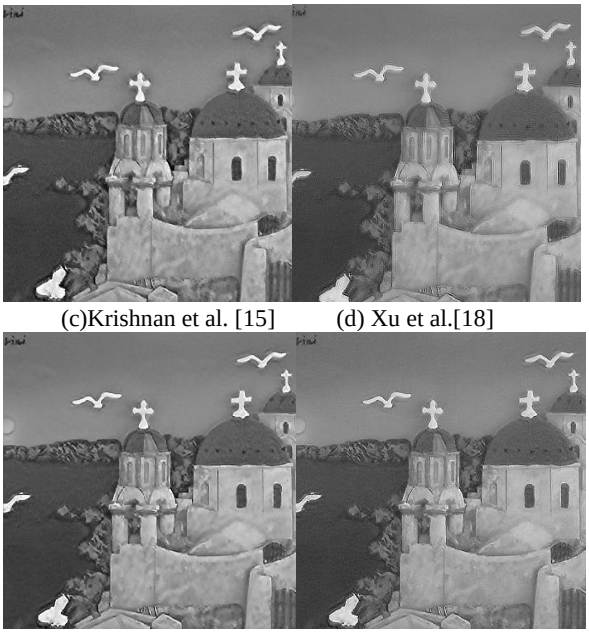

(c)Krishnan et al. [15] (d) Xu et al.[18]

(e) Pan et al .[19] (f)Ours

Fig.6 Deblurred results of image "house" using differrent methods

In Fig.7, we choose a challenging image example that was used in [8] which has dense edges and details with a big blurring kernel, in order to show the deblurring ability of different methods. The results of [20] and [15] show obvious blurring and ringing effect, while the results of [18] have some small ringing effects. The Results of [19] and our proposed method show relatively clear boundaries and clearer letters in the image. The NIQE evaluation results shown in Table6 are in accordance with the above analyses, since our proposed method has a higher NIQE value than [20], [15] and [18] and a comparably value of [19]. However, the method utilized in [19] is time consuming, which usually need several minutes to process. Thus, our proposed method is more effective and convenient.

We should add that the proposed approach has been tried on many other real-world motion blurred images with the parameter settings suggested in this paper, most of which are deblurred with visually plausible perception.

(a)Blurred image (b) Bioucas-Dias et al.[20]

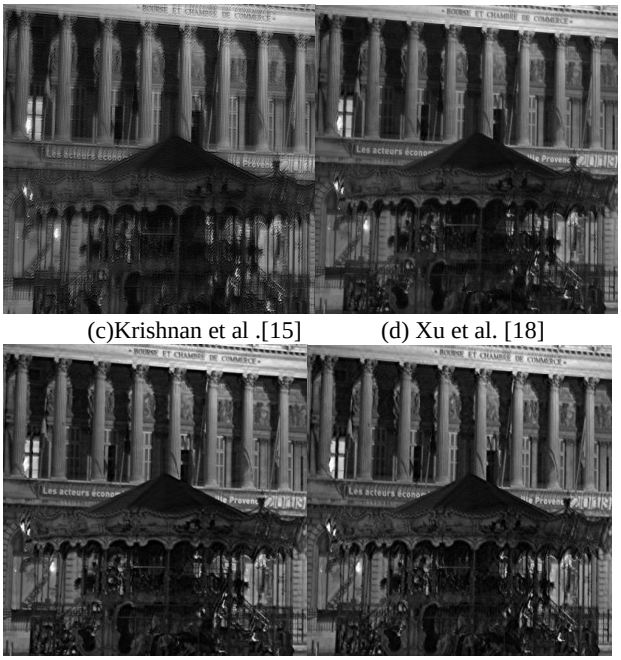

(c)Krishnan et al .[15] (d) Xu et al. [18]

(e) Pan et al. [19] (f)Ours

Fig.7 Deblurred results of image "Building" using differrent methods

V. Conclusion

In this paper, we propose a new motion deblurring method by combining global prior, sparse representation and kernel constraint in a unified framework, which is then transferred to an optimization problem. We alternately solve the variables to obtain the estimated kernel and deblurred image. To get an accurate kernel, we propose an edge selection method for selecting useful edges and introduce an intermediate image to acquire precise results.

Experimental results show that the proposed method runs fast and achieves comparable performance to state-of-the-art algorithms, sometimes even outperforms them in both synthetic and real-world image experiments.

References

[1] Fergus, R., Singh, B., Hertzmann, A., Roweis, S.T., Freeman, W.T.: Removing camera shake from a single photograph. ACM Trans. Graph. 25(3), 787-794 (2006).

[2] Shan Q, Jia J, Agarwala A. High-quality motion deblurring from a single image[J].ACM Trans. Graph, 2008,27(3):1-10.

[3] Krishnan D, Fergus R. Fast image deconvolution using hyper-Laplacian priors. In NIPS[C]// Advances in Neural Information Processing Systems 22: Conference on Neural Information Processing Systems 2009. Proceedings of A Meeting Held 7-10 December 2009, Vancouver, British Columbia, Canada. DBLP, 2009:1033-1041.

[4] D. Geman and G. Reynolds. Constrained restoration and recovery of discontinuities. PAMI,14(3):367– 383, 1992.

[5] D. Geman and C. Yang. Nonlinear image recovery with half-quadratic regularization. PAMI,4:932– 946, 1995.

[6] Zhang X, Wang R, Tian Y, et al. Image deblurring using robust sparsity priors[C]// IEEE International Conference on Image Processing. IEEE, 2015:138-142.

[7] Cho S, Lee S. Fast motion deblurring[J]. Acm Transactions on Graphics, 2009, 28(5):1-8.

[8] Xu L, Jia J. Two-Phase Kernel Estimation for Robust Motion Deblurring[C]// Computer Vision - ECCV 2010, European Conference

on Computer Vision, Heraklion, Crete, Greece, September 5-11, 2010, Proceedings. DBLP, 2010:157-170.
[9] Joshi N, Szeliski R, Kriegman D J. PSF estimation using sharp edge prediction[C]// IEEE Computer Society Conference on Computer Vision and Pattern Recognition. DBLP, 2008:1-8.
[10] Lei Li, Ruiting Zhang, Jiangming Kan, Wenbin Li. Image deblurring via an adaptive dictionary learning strategy [J]. Telkomnika, 2014, Vol.12 (4): 855-864.
[11] Yin M, Gao J, Tien D, et al. Blind image deblurring via coupled sparse representation[J]. Journal of Visual Communication & Image Representation, 2014, 25(5):814-821.
[12] Elad M, Aharon M. Image Denoising Via Sparse and Redundant Representations Over Learned Dictionaries[J]. IEEE Transactions on Image Processing A Publication of the IEEE Signal Processing Society, 2006, 15(12):3736-45.
[13] Jia C, Evans B L. Patch-based image deconvolution via joint modeling of sparse priors[C]// IEEE International Conference on Image Processing, ICIP 2011, Brussels, Belgium, September. DBLP, 2011:681-684.
[14] Xu L, Jia J. Two-phase kernel estimation for robust motion deblurring[C]// Computer Vision - ECCV 2010, European Conference on Computer Vision, Heraklion, Crete, Greece, September 5-11, 2010, Proceedings. DBLP, 2010:157-170.
[15] Krishnan D, Tay T, Fergus R. Blind deconvolution using a normalized sparsity measure[C]// IEEE Conference on Computer Vision and Pattern Recognition. IEEE Computer Society, 2011:233-240.
[16] Efron B, Hastie T, Johnstone I, et al. Least Angle Regression[J]. Annals of Statistics, 2004, 32(2):407-451.
[17] Jia C, Evans B L. Patch-based image deconvolution via joint modeling of sparse priors[C]// IEEE International Conference on Image Processing, ICIP 2011, Brussels, Belgium, September. DBLP, 2011:681-684.
[18] Xu L, Zheng S, Jia J. Unnatural L0 Sparse Representation for Natural Image Deblurring[C]// Computer Vision and Pattern Recognition. IEEE, 2013:1107-1114.
[19] Pan J, Liu R, Su Z, et al. Kernel estimation from salient structure for robust motion deblurring[J]. Signal Processing Image Communication, 2013, 28(9):1156-1170.
[20] Bioucas-Dias J M, Figueiredo M A T, Oliveira J P. Total Variation-Based Image Deconvolution: a Majorization-Minimization Approach[C]// IEEE International Conference on Acoustics, Speech and Signal Processing, 2006. ICASSP 2006 Proceedings. IEEE, 2006: II-II.
[21] Lai W S, Huang J B, Hu Z, et al. A Comparative Study for Single Image Blind Deblurring[C]// IEEE Conference on Computer Vision and Pattern Recognition. IEEE, 2016:1701-1709.
[22] Mittal A, Soundararajan R, Bovik A C. Making a “Completely Blind” Image Quality Analyzer[J]. IEEE Signal Processing Letters, 2013, 20(3):209-212.

Xixuan Zhao born in 1992, received her Bachelor's degree from China Jiliang University, Hangzhou, China, at 2011~2015. Now she is pursuing her doctoral degree at Beijing Forestry University, Beijing, China. Her research interests include image processing and computer vision

Jiangming Kan born in 1976, Ph.D. degree, professor at Beijing Forestry. His research interests include computer vision and intelligent control.